

# Visible light photodegradation of rhodamine B over VDF/CTFE copolymer-templated crystalline mesoporous titania

Guoli Zi · Yi Wang · Kai Zheng · Huan Zhao ·  
Fuzhi Wang · Wenjun Zhang · Zhiying Yan ·  
Jiao He · Jiaqiang Wang

Received: 7 January 2012 / Accepted: 2 April 2012 / Published online: 25 April 2012  
© Springer Science+Business Media B.V. 2012

**Abstract** Mesoporous TiO<sub>2</sub> with anatase crystalline structure (MTiO<sub>2</sub>/F<sub>2319</sub>) has been synthesized by using vinylidene fluoride/chlorotrifluoroethylene copolymer (1:9 in mole, F<sub>2319</sub>) as template. The synthesized mesoporous titania samples were characterized by a combination of various physicochemical techniques, such as X-ray diffraction, scanning electron microscopy, high-resolution transmission electron microscopy, and N<sub>2</sub> adsorption/desorption. It was found that without any external doping, MTiO<sub>2</sub>/F<sub>2319</sub> exhibited significantly higher photocatalytic activities for the degradation of rhodamine B (RhB) dye than P25 TiO<sub>2</sub> under visible light irradiation. Furthermore, the UV-Vis absorption maximum of the dye solution exhibited a gradual hypsochromic shift due to de-ethylation and degradation of RhB dye.

**Keywords** Crystalline mesoporous TiO<sub>2</sub> · Visible light photocatalysis · F<sub>2319</sub> copolymer · Rhodamine B

## Introduction

Photocatalytic processes involving TiO<sub>2</sub> semiconductor particles under UV light illuminations have been shown to be potentially advantageous and useful in the treatment of wastewater pollutants [1]. However, TiO<sub>2</sub> requires UV light for photoreactions to proceed. This greatly limits the use of sunlight as an energy source for the photoreactions, because sunlight is comprised of less than 5 % ultraviolet light. To develop more light-efficient catalysts, there is an urgent need to develop photocatalytic systems that are able to operate effectively under solar light irradiation

---

G. Zi · Y. Wang · K. Zheng · H. Zhao · F. Wang · W. Zhang · Z. Yan · J. He · J. Wang (✉)  
Department of Applied Chemistry, The Universities' Center for Photocatalytic Treatment of  
Pollutants in Yunnan Province, Yunnan University, Kunming 650091, People's Republic of China  
e-mail: jqwang@ynu.edu.cn

[2, 3]. Due to the direct correlation between the photocatalytic performance and the microstructure of a semiconductor photocatalyst, searching for new photocatalysts with an appropriate crystal structure has been the intensively pursued topic in heterogeneous photocatalysis [4]. It is well known that the effectiveness of  $\text{TiO}_2$  photocatalyst is very sensitive to its crystallinity, particle size, and crystal phase [5], and mesoporous  $\text{TiO}_2$  has been shown to be potentially advantageous because it shows higher surface areas, much more uniform and controllable pore size, and pore morphologies compared to randomly organized nanocrystalline  $\text{TiO}_2$  [6]. For example, poorly crystalline nanoparticles can result in limited photocatalytic effects since the defects in  $\text{TiO}_2$  can act as recombination sites of generated electrons ( $e^-$ ) and holes ( $h^+$ ) [7], while single-crystalline  $\text{TiO}_2$  provides rapid electron transfer with high efficiency [8]. Therefore, one of the strategies of making highly active  $\text{TiO}_2$  is to give particle high crystallinity, which may reduce the possibility of electron–hole pairs recombination at a defective site [5]. At the same time, anatase is the preferred phase of  $\text{TiO}_2$  with catalytic effects superior to other phases [9]. Nevertheless, the fabrication of crystalline mesoporous  $\text{TiO}_2$  is not easy to succeed because of the sensitivity of the structure toward the heat-treatment procedure and crystallization [10]. We successfully synthesized mesoporous  $\text{TiO}_2$  materials with an anatase crystalline framework to retain their structural integrity and mesoporosity when calcined at 773 K.

Up to now, the general synthetic strategies for mesoporous  $\text{TiO}_2$  have been developed using a variety of templates, such as phosphates amine, ionic surfactants, block polymer, nonionic surfactants, and nonsurfactant templates [5, 11–15]. However, both templates and dopants are essential for the synthesis of visible-light photocatalysts based on mesoporous  $\text{TiO}_2$ . Recently, in our group, 14 commercial synthetic dyes were directly used as structure-directing agents that convert to carbonaceous materials after calcination in synthesis of thermally stable meso-structured  $\text{TiO}_2$  [12]. Without any external doping, this in situ carbon enhanced the visible light photocatalytic activities for the degradation of aqueous dyes. In this paper, we have extended our previous work on dye templates to a new block copolymer template ( $F_{2319}$ ). We also want to obtain visible-light photocatalytic activity without any external doping by using  $F_{2319}$  as a template for the preparation of mesoporous  $\text{TiO}_2$ .

Vinylidene fluoride/chlorotrifluoroethylene (VDF/CTFE) random copolymers are synthesized by copolymerizing VDF with CTFE in different molar ratios.  $F_{2319}$  has much higher decomposition temperature than those fluoride-free copolymers such as P123 ( $\text{EO}_{20}\text{PO}_{70}\text{EO}_{20}$ ). The molecular weight of the  $F_{2319}$  polymer we used was  $\sim 3.0 \times 10^5$  g/mol. Recently, grafted VDF/CTFE polymers have been used as templates to synthesize  $\text{TiO}_2$  thin films [16] and Ag-loaded  $\text{TiO}_2$  nanostructures [17] through a sol–gel process. However, hydrothermal synthesis of mesoporous  $\text{TiO}_2$  using pure VDF/CTFE random polymers as template has not been investigated as far as we know. In particular, previous studies have not yet addressed the direct use of  $F_{2319}$  as a template in the synthesis of thermally stable crystalline mesoscopic ordering and visible-light photocatalytic activity.

Herein we report on the synthesis and characterization of mesoporous  $\text{TiO}_2$  with an anatase crystalline structure ( $\text{MTiO}_2/\text{F}_{2319}$ ) templated by a VDF/CTFE

random copolymer, i.e., VDF/CTFE copolymer with a 1:9 molar ratio (F<sub>2319</sub>). MTiO<sub>2</sub>/F<sub>2319</sub> exhibited significant visible light photocatalytic activity without any external doping.

## Experimental

### Synthesis

In a typical preparation process, 1.0 g F<sub>2319</sub> ([(-CF<sub>2</sub>-CH<sub>2</sub>-)<sub>a</sub>-(-CF<sub>2</sub>-CFCl-)<sub>b</sub>]<sub>m</sub>, a:b = 1:9) copolymer was put into 90 mL of ethyl acetate, and an ultrasonic treatment for more than a week was carried out to help F<sub>2319</sub> copolymer dissolve. Afterwards, 10 mL of distilled water was added slowly into the supernatant, and then 8 mL of tetrabutyl titanate was added drop-wise under continuous stirring. Subsequently, the mixture was stirred for 24 h and then transferred into a Teflon bottle and treated under autogenous pressure at 363 K for 7 days, filtered, washed, and then dried. Finally, the sample was calcined in air at 773 K for 8 h and then a powder was obtained.

### Characterizations

X-ray powder diffraction (XRD) experiments were conducted on a D/max-3B spectrometer with Cu K $\alpha$  radiation. Scans were made in the  $2\theta$  range 5–90° with a scan rate of 10°/min (wide-angle diffraction). Pore size distributions, BET surface areas, and pore volumes were measured by nitrogen adsorption/desorption using a Micromeritics Tristar II Surface Area and Porosity Analyzer. Prior to the analysis, the samples were degassed at 150 °C for 1 h. Scanning electron microscopy (SEM) images were taken on an FEI Quanta200 FEG microscope at an accelerating voltage of 15 kV with the pressure in the sample chamber of 1 Torr. High-resolution transmission electron microscopy (HRTEM) images were taken on a TEM (TECNAI G<sup>2</sup> S-TWIN F20).

### Photocatalytic activity

The reaction of the photocatalytic degradation of rhodamine B (RhB, C<sub>28</sub>H<sub>31</sub>ClN<sub>2</sub>O<sub>3</sub>) was carried out in a glass beaker containing 50 mL of a model solution (10 ppm) and 25 mg of photocatalyst. The suspensions were magnetically stirred in dark for 24 h to attain adsorption–desorption equilibrium between dye and mesoporous TiO<sub>2</sub>. After the system reached the adsorption–desorption equilibrium and dissolved oxygen, they were exposed for 5 h under visible light. The photocatalytic experiments were carried out under visible light with an 800-W Xe-illuminator in which a colored glass filter ( $\lambda > 420$  nm) was utilized for the purpose of allowing only visible radiation. Laboratorial film was used to seal the beaker so that the volume of the solutions decreased little after the experiment. The solutions were mixed with a magnetic stirrer during the reaction process. The concentration of residual RhB was measured at an interval of 1 h by monitoring

UV-Vis spectrum over 200–800 nm after centrifugation at 2,500 rpm for 10 min and subsequently filtered through a Millipore filter (pore size, 0.45  $\mu\text{m}$ ). All the absorbance-concentration standard curves were obtained using this apparatus. The determination wavelength is 553 nm, which is the maximum absorption wavelength of RhB as detected by UV-Vis spectrometer. The decrease due to adsorption can be deducted after the adsorption equilibrium was achieved. Therefore, photodegradation yield is defined as: [18]

$$\text{photodegradation yield} = \frac{C_o - C_a - C_b}{C_o} \times 100\% \quad (1)$$

$C_o$  is the initial concentration of dye,  $C_a$  is the concentration after photodegradation of dye, and  $C_b$  is the decrease concentration because of the direct photolysis.

## Results and discussion

### Synthesis of mesoporous $\text{TiO}_2$

In order to use  $F_{2319}$  copolymer as template in a hydrothermal process, it had to be dissolved in an appropriate solvent.  $F_{2319}$  copolymer is difficult to dissolve in ordinary solvents such as absolute ethyl alcohol, frequently used in a hydrothermal process. Therefore, ethyl acetate was used as solvent and a long-term ultrasonic treatment was also employed. In addition, the  $F_{2319}$  copolymer can serve as a scaffold for the mesostructure in titania crystallization before they decompose at  $\sim 723$  K. This temperature is much higher than the decomposition temperature of traditional PEO-based block copolymer such as F127 and P123 templates ( $\sim 523$  K) [19]. Therefore, a high temperature of 773 K was employed in order to remove the template completely, higher than ordinary calcination temperature (up to 673 K) in a typical process of anatase  $\text{TiO}_2$  synthesis. The high calcinations temperature implies that the synthesized mesoporous  $\text{TiO}_2$  has a high thermal stability.

### The characterizations of photocatalyst

Figure 1 shows the  $\text{N}_2$  adsorption/desorption isotherm and BJH pore-size distribution plots (inset) of  $\text{MTiO}_2/\text{F}_{2319}$ . Typical IV adsorption/desorption isotherm is observed, which indicates the mesoporous structure of prepared material. This phenomenon is in good agreement with those mesoporous  $\text{TiO}_2$  templated by other traditional templates, such as block copolymers or surfactants. The specific surface area, pore volume, and average pore diameter of  $\text{MTiO}_2/\text{F}_{2319}$  were 61.7  $\text{m}^2/\text{g}$ , 0.15  $\text{cc}/\text{g}$ , and 9.0 nm, respectively. The surface area of the as-synthesized sample was similar to that of mesoporous  $\text{TiO}_2$  films templated by P123 block copolymer (58  $\text{m}^2/\text{g}$ ) [20], but lower than by F127 block copolymer (122  $\text{m}^2/\text{g}$ ) [21]. This could be attributed to the use of different templates and the higher calcination temperatures. The BJH pore-size distribution of  $\text{MTiO}_2/\text{F}_{2319}$  indicates that the catalysts have regular mesoporous channels.

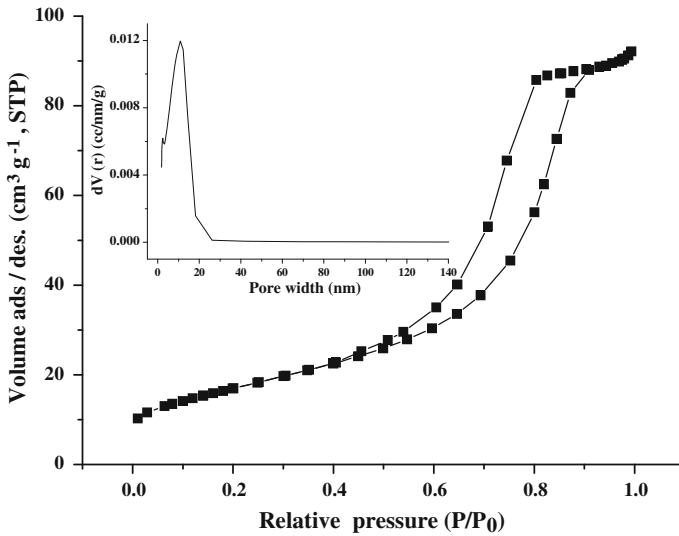


**Fig. 1** N<sub>2</sub> adsorption/desorption isotherm and BJH pore-size distribution (*inset*) of MTiO<sub>2</sub>/F<sub>2319</sub>

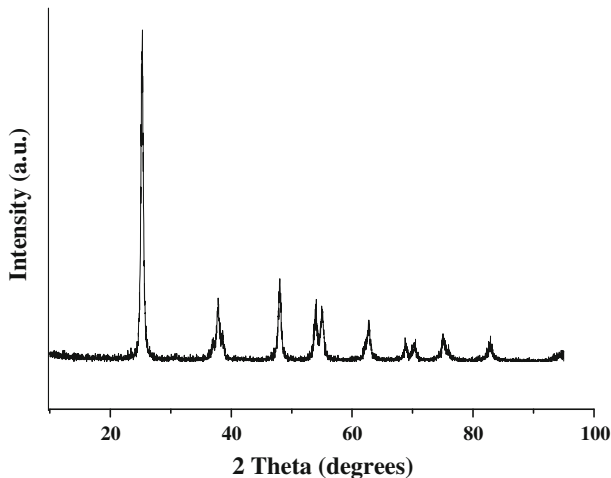


**Fig. 2** X-ray diffraction pattern of MTiO<sub>2</sub>/F<sub>2319</sub>

XRD pattern of MTiO<sub>2</sub>/F<sub>2319</sub> is shown in Fig. 2. Several diffraction peaks, which are well-matched with the diffraction patterns of anatase TiO<sub>2</sub>, are observed in the wide-angle diffraction region. It can be clearly seen that the diffraction peaks are sharp and intensive, suggesting the formation of MTiO<sub>2</sub>/F<sub>2319</sub> crystals with only one pure crystalline phase present, namely anatase. This again suggests that F<sub>2319</sub> polymer template has a high-temperature decomposition-resistant character and inhibited phase transition from anatase to other phase in the process of crystallization.

The average size of anatase nanocrystals calculated by the Scherrer equation is to be  $\sim 20$  nm.

SEM and high-resolution TEM images of  $\text{MTiO}_2/\text{F}_{2319}$  are shown in Fig. 3a, b, and c, respectively. SEM reveals that this sample has no regular morphology and highly aggregated (Fig. 3a). The crystallinity of anatase phase in the mesoporous wall is observed from the HRTEM images of  $\text{MTiO}_2/\text{F}_{2319}$ . Figure 3b shows that the highly aggregated nanocrystal composed of disordered primary nanoparticles (20–30 nm in size), which is in agreement with the domain size (ca. 20 nm) obtained from XRD by applying the Scherrer equation. The synthesis of well-crystallized particles with mesoporous wall in the literature was limited. Figure 3c shows clear lattice fringes. It also clearly confirmed that the mesoporous  $\text{TiO}_2$  are highly crystalline and almost no amorphous structures can be observed. The crystalline framework enables the superior performance of photocatalytic activities for the degradation of RhB dye.

### Photocatalytic activity

In photocatalytic experimentation, after reaching the adsorption equilibrium, the variations for the concentrations of the studied materials are summarized in Fig. 4. The photodegradation yields using  $\text{MTiO}_2/\text{F}_{2319}$  and P25  $\text{TiO}_2$  as photocatalysts are included. The photodegradation yield of RhB in the presence of the  $\text{MTiO}_2/\text{F}_{2319}$  can be up to 71.4 % under visible light, while P25  $\text{TiO}_2$  only had 55.4 % under visible light (Table 1). The degradation of RhB on P25  $\text{TiO}_2$  under visible light irradiation can be attributed to the self-sensitization of RhB since RhB served as sensitizer in the process of dye sensitized  $\text{TiO}_2$  photocatalysis [22]. More importantly, it is obvious that  $\text{MTiO}_2/\text{F}_{2319}$  composite exhibited higher photocatalytic activity under visible light ( $\lambda > 420$  nm) than P25  $\text{TiO}_2$  although the photodegradation yield of  $\text{MTiO}_2/\text{F}_{2319}$  and P25  $\text{TiO}_2$  increased with increasing reaction time. Therefore,  $\text{MTiO}_2/\text{F}_{2319}$  had apparently better visible photocatalysis than P25  $\text{TiO}_2$ .

The variation of UV-Vis spectra of RhB during photodegradation over  $\text{MTiO}_2/\text{F}_{2319}$  under visible light ( $\lambda > 420$  nm) is shown in Fig. 5. It is seen that the absorption peaks corresponding to RhB diminished under visible light irradiation

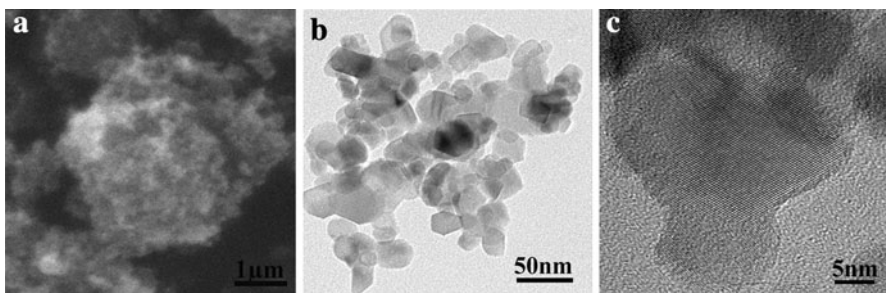


**Fig. 3** SEM (a), HRTEM images (b–c) of  $\text{MTiO}_2/\text{F}_{2319}$

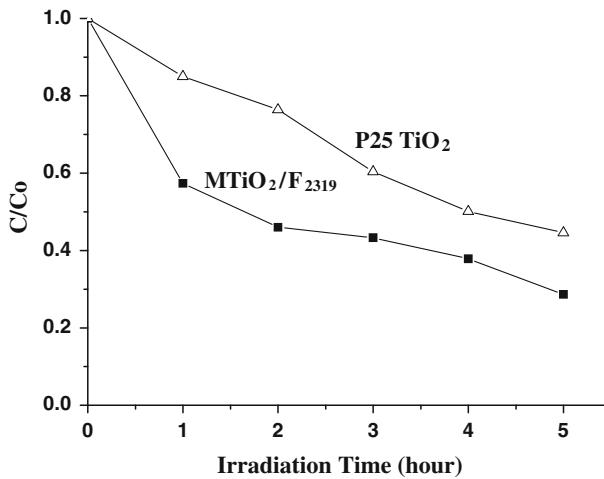


**Fig. 4** Comparison of photodegradation yields of rhodamine B over MTiO<sub>2</sub>/F<sub>2319</sub> and Degussa P25 TiO<sub>2</sub> under visible light irradiation ( $\lambda > 420$  nm)

**Table 1** Photocatalytic activities of MTiO<sub>2</sub>/F<sub>2319</sub> and P25 TiO<sub>2</sub> under visible light ( $\lambda > 420$  nm) in different reaction times (%)

Catalysts	Photodegradation yield of RhB (%) under visible light ( $\lambda > 420$ nm)				
	1 h	2 h	3 h	4 h	5 h
MTiO <sub>2</sub> /F <sub>2319</sub>	42.7	54.0	56.7	62.1	71.4
P25 TiO <sub>2</sub>	15.0	23.6	39.6	49.9	55.4

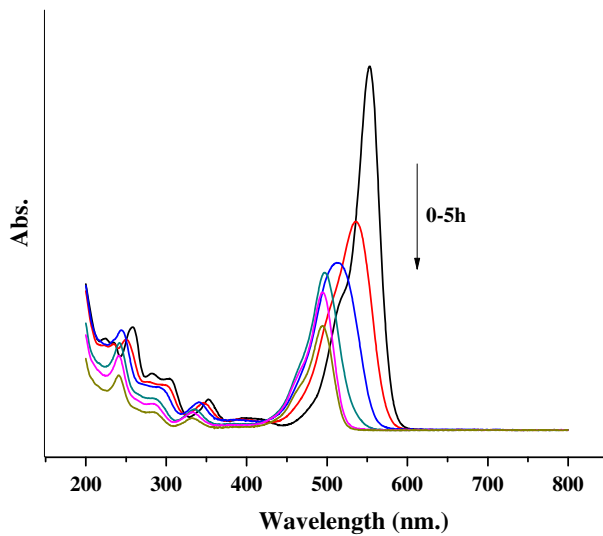
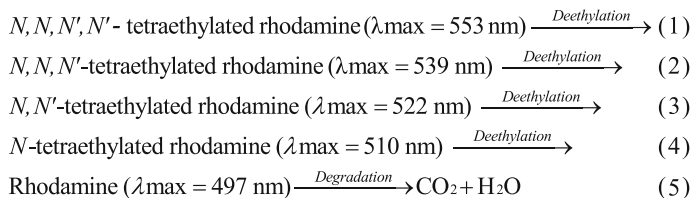


**Fig. 5** UV-Vis spectra of RhB during photodegradation over MTiO<sub>2</sub>/F<sub>2319</sub> at different times under visible light irradiation ( $\lambda > 420$  nm)



**Scheme 1** De-ethylation and degradation processing of *N,N,N',N'*-tetraethylated rhodamine (RhB) molecule

and indicate the degradation of RhB. No new absorption bands, especially, the absorption bands of aromatic moieties and other similar intermediates, were observed. Besides, visible light irradiation of the aqueous RhB-MTiO<sub>2</sub>/F<sub>2319</sub> dispersion leads to a wavelength shift of the band to shorter wavelengths accompany with decrease in absorption. In general, the spectral shift from 553 nm with a concomitant diminishing of absorption peaks during 5 h. The wavelength shift depicted in Fig. 5 is caused by de-ethylation of RhB because of attack by one of the active oxygen species on the *N*-ethyl group [4]. De-ethylation of the fully *N,N,N',N'*-tetraethylated rhodamine molecule (i.e., RhB) has the wavelength position of its major absorption band moved toward the blue region (Scheme 1(1–4)) [4, 23]. When the de-ethylated process is fully completed, the absorption band shifts to 497 nm and RhB is turned to rhodamine. Rhodamine is then gradually decomposed due to the further destruction of the conjugated structure (Scheme 1(5)) [23, 24].

The above results are analogous to those of the competitive photodegradation reactions between the polyoxyethylene chain and the aromatic ring in polyoxyethylated nonylphenol. During the initial period of photodegradation of RhB, competitive reactions between de-ethylation and cleavage of the RhB chromophore ring structure occur, with de-ethylation predominating. Irradiation by visible light for longer periods of time leads to further decomposition of the de-ethylated rhodamine intermediates as indicated by changes in peak intensity at 497 nm (Fig. 5) [4, 25].

The formation of large-pore mesoscopically ordered titania oxides via such a simple procedure suggests that the F<sub>2319</sub> moleculars are the ideal building blocks for synthesis of visible light photocatalysts, even though F<sub>2319</sub> moleculars are expected to behave in a more complex manner than those conventional PEO-based block copolymer templates. It is also interesting to evoke some reasons why the mesoporous titanium dioxides prepared by using F<sub>2319</sub> as template exhibited visible light photocatalytic activities. Obviously, the crystalline framework, large pore size, and high thermal stability of these new mesoporous titanias are expected to afford better activity toward photocatalytic reactions. Indeed, mechanism details of the formation of mesoporous materials are still far from understood.

## Conclusions

In summary, F<sub>2319</sub> were successfully used as template to synthesize mesoporous anatase crystalline TiO<sub>2</sub>. The synthesized MTiO<sub>2</sub>/F<sub>2319</sub> sample without any external

doping exhibited higher photocatalytic activity for the degradation of RhB under visible light irradiation than P25 TiO<sub>2</sub>. Both de-ethylation and degradation of RhB take place under visible light irradiation in the presence of MTiO<sub>2</sub>/F<sub>2319</sub> particles. We believe that the synthetic strategy demonstrated here could also be extended to other mesoporous materials with visible-light photocatalytic activity, such as, SiO<sub>2</sub> and Al<sub>2</sub>O<sub>3</sub> and other photosensitizing agents studies of which are ongoing.

**Acknowledgments** The authors thank the Natural Science Foundation of China (Project NSFC-YN U1033603, 20863009, 21063016.), Yunnan Province (Project 20008CD065), Specialized Research Fund for the Doctoral Program of Higher Education (200806730005), Program for Innovative Research Team (in Science and Technology) in University of Yunnan Province (IRTSTYN) the R&D Program of Kunming (11H-011101, 2011-15) for financial support.

## References

1. M. Saquib, M. Muneer, *Dyes Pigment.* **56**, 37 (2003)
2. C. Chen, X. Li, W. Ma, J. Zhao, H. Hidaka, N. Serpone, *J. Phys. Chem. B* **106**, 318 (2002)
3. R. Asahi, T. Morikawa, T. Ohwaki, K. Aoki, Y. Taga, *Science* **293**, 269 (2001)
4. T. Wu, G. Liu, J. Zhao, H. Hidaka, N. Serpone, *J. Phys. Chem. B* **102**, 5845 (1998)
5. Y. Yue, Z. Gao, *Chem. Commun.* **18**, 1755 (2000)
6. A. Hagfeldt, M. Grätzel, *Chem. Rev.* **95**, 49 (1995)
7. J. Seo, H. Chung, M. Kim, J. Lee, I. Choi, J. Cheon, *Small* **3**, 850 (2007)
8. M. Adachi, Y. Murata, J. Takao, J. Jiu, M. Sakamoto, F. Wang, *J. Am. Chem. Soc.* **126**, 14943 (2004)
9. Z. Ding, G. Lu, P. Greenfield, *J. Phys. Chem. B* **104**, 4815 (2000)
10. B. Smarsly, D. Grosso, T. Brezesinski, N. Pinna, C. Boissière, M. Antonietti, C. Sanchez, *Chem. Mater.* **16**, 2948 (2004)
11. P. Yang, D. Zhao, D. Margolese, B. Chmelka, G. Stucky, *Chem. Mater.* **11**, 2813 (1999)
12. J. Wang, J. Wang, Q. Sun, W. Wang, Z. Yang, W. Gong, L. Min, *J. Mater. Chem.* **19**, 6597 (2009)
13. D. Antonelli, J. Ying, *Angew. Chem. Int. Ed.* **34**, 2014 (1995)
14. E. Crepaldi, G. Soler-Illia, D. Grosso, F. Cagnol, F. Ribot, C. Sanchez, *J. Am. Chem. Soc.* **125**, 9770 (2003)
15. J. Koh, J. Seo, J. Park, J. Kim, *J. Colloid Interface Sci.* **338**, 486 (2009)
16. J. Koh, J. Seo, S. Ahn, J. Kim, *Thin Solid Films* **519**, 158 (2010)
17. J. Koh, J. Seo, J. Koh, J. Kim, *Mater. Lett.* **63**, 1360 (2009)
18. F. Xia, E. Ou, L. Wang, J. Wang, *Dyes Pigment.* **76**, 76 (2008)
19. B. Ma, J. Ma, G. Goh, *J. Mater. Sci.* **43**, 4297 (2008)
20. C. Wu, T. Ohsuna, M. Kuwabara, K. Kuroda, *J. Am. Chem. Soc.* **128**, 4544 (2006)
21. X. Meng, T. Kimura, T. Ohji, K. Kato, *J. Mater. Chem.* **19**, 1894 (2009)
22. W. Ren, Z. Ai, F. Jia, L. Zhang, X. Fan, Z. Zou, *Appl. Catal. B Environ.* **69**, 138 (2007)
23. D. Zhang, Y. Mo, L. Song, X. Huang, R. Qiu, *Chin. J. Process Eng.* **8**, 78 (2008)
24. J. Bi, L. Wu, J. Li, Z. Li, X. Wang, X. Fu, *Acta Mater.* **55**, 4699 (2007)
25. E. Peitzelt, C. Minero, V. Maurino, A. Sciafani, H. Hidaka, N. Serpone, *Environ. Sci. Technol.* **23**, 1380 (1989)